Eur. Phys. J. B **1**, 439–452 (1998)

THE EUROPEAN PHYSICAL JOURNAL B

Interplay between chains of S = 5/2 localised spins and two-dimensional sheets of organic donors in the synthetically built magnetic multilayer $\lambda-(BETS)_2FeCl_4$

L. Brossard[1,a], R. Clerac[2], C. Coulon[2], M. Tokumoto[3], T. Ziman[4], D.K. Petrov[5,b], V.N. Laukhin[5,6,c], M.J. Naughton[5], A. Audouard[1], F. Goze[1], A. Kobayashi[7], H. Kobayashi[8], and P. Cassoux[9]

[1] Laboratoire de Physique de la Matière Condensée[d], SNCMP, INSA, Complexe Scientifique de Rangueil, 31077 Toulouse Cedex, France
[2] Centre de Recherches Paul Pascal, CNRS, avenue du Dr. Schweitzer, 33600 Pessac, France
[3] Electrotechnical Laboratory, Tsukuba, Ibaraki 305, Japan
[4] Laboratoire de Physique Quantique[e], IRSAMC, Université P. Sabatier, route de Narbonne, 31062 Toulouse Cedex, and Institut Laue Langevin, BP 156, 38042 Grenoble Cedex 9, France
[5] Department of Physics, State University of New York, Buffalo, New York 14260, USA
[6] Institute of Chemical Physics, Russian Academy of Sciences, Chernogolovka 142432, Russia
[7] Department of Chemistry, Faculty of Science, The University of Tokyo, Hongo, Bunkyo-ku, Tokyo 113, Japan
[8] Institute for Molecular Science, Nishigo-naka 38, Myodaiji, Okasaki 444, Japan
[9] Laboratoire de Chimie de Coordination, CNRS, 205 route de Narbonne, 31077 Toulouse Cedex, France

Received: 6 August 1997 / Received: 5 November 1997 / Accepted: 10 November 1997

Abstract. In order to understand the magnetic field-induced restoration of a highly conductive state in $\lambda-(BETS)_2FeCl_4$, static (SQUID) and dynamic (ESR and AFR) magnetization measurements were performed on polycrystalline samples and single crystals, respectively. In addition, cantilever and resistivity measurements under steady fields were performed. While the metal-insulator transition curve of the (T, B) phase diagram exhibits a first order character, a "spin-flop" transition line divides the insulating state when the magnetic field is applied along the easy axis of magnetization. The effects of a RKKY-type indirect exchange and of applied magnetic field are described within the framework of a generalized Kondo lattice, namely two chains of $S = 5/2$ Fe^{3+} localised spins coupled through the itinerant spins of the 2D sheets of BETS. The calculations, which can incorporate intramolecular electron correlations within a mean field theory, are in qualitative agreement with the field induced transition from the antiferromagnetic insulating ground state to a canted one, *i.e.* a not fully oriented paramagnetic, but metallic state.

PACS. 71.30.+h Metal-insulator transitions and other electronic transitions – 75.30.Kz Magnetic phase boundaries (including magnetic transitions metamagnetion, etc.) – 75.30.Fv Spin density waves

1 Introduction

Due to the low dimensionality of organic conductors, the electron gas of these compounds are known to display a very rich spectrum of instabilities [1]. These instabilities may be induced by various parameters and lead to either metal-semimetal or metal-insulator transitions, depending on the amount of Fermi surface (FS) involved in the electron-hole condensation. These phase transitions are associated with a great variety of ground states, either spin-Peierls and charge density wave (CDW), or spin density wave (SDW) and superconductivity. Competition between the two latter ground states constitutes a still appealing question.

Charge transfer salts based upon donor molecules BEDT-TTF (bis(ethylenedithio)-tetrathiafulvalene, also designated as ET) have been shown to develop S$\cdots$S intermolecular interactions and thus display quasi one-dimensional (1D) and two-dimensional (2D) electron properties. In order to enhance the 2D character, replacement of the sulphur atoms in the fulvalene moiety of ET by selenium atoms led to the study of bis(ethylenedithio)-tetraselenafulvalene (BETS) salts [2]. A number of organic-inorganic hybrid salts based on BETS with several anions and exhibiting various so-called $\lambda-$, $\kappa-$, and $\theta-$type

[a] e-mail: brossard@insa-tlse.fr
[b] *Present address*: IBM, T.J. Watson Research Center, Yorktown Heights, N.Y. 10598, USA.
[c] *Present address*: Institut de Ciencia de Materials, CSIC, Campus de la UAB, 08193 Bellaterra, Spain.
[d] UMR CNRS 5830
[e] UMR CNRS 5626

molecular arrangements have been prepared and characterized [3–10].

Within this series of salts, the $\lambda-(BETS)_2MCl_4$ compounds with M = Fe, Ga are of special interest since linear chains of $[M(III)Cl_4]^-$ anions are intercalated between the 2D conducting sheets containing the BETS molecules. Whereas $\lambda-(BETS)_2FeCl_4$ becomes insulating below 8.5 K [7], its gallium analogue is superconducting below 8 K [6,11]. The $\lambda-(BETS)_2Ga_{1-x}Fe_xCl_4$ mixed anion system also undergoes a superconducting transition at temperatures decreasing from 8 K to 3.5 K as x increases from 0 to 0.5 [12]. This last result is similar to that observed in the $(ET)_4M(C_2O_4)_3(H_2O)C_6H_5CN$ salts which become superconducting below $T_c = 7$ K [13] and 5 K [14] with M = Fe^{3+} and Cr^{3+}, respectively. In that case, linear chains of magnetic ions M^{3+} with respective spin values $S = 5/2$ and $3/2$, are also intercalated between the (super) conductive sheets of ET molecules. Within the BCS weak coupling scheme, these magnetic ions should destroy superconductivity in their nearest proximity, which should yield a 2D character of the superconducting gap. These results also raise the question of the nature of the superconductive coupling in these organic compounds. Is the Cooper pairing between electrons phonon-mediated or not? And if it is, up to which level of oscillator forces are the intra- and inter-molecular modes of the donor vibrations respectively involved? On the other hand, should the superconducting phase occur in the immediate vicinity of an antiferromagnetic (AF) SDW state within the phase space as in the case of the quasi-1D $(TMTSF)_2X$ Bechgaard salts [15], then the coupling is likely to be electron-mediated due to rather large electron-electron scatterings. Whereas this conclusion is asserted from the pressure-temperature phase diagram of some $(TMTSF)_2X$ salts [15], competition between superconductivity and a possible AF state can now be studied within the series of isostructural $\lambda-(BETS)_2Ga_{1-x}Fe_xCl_4$ compounds. In this case, pressure effects could be chemically induced, although in the presence of possible random disorder between the Fe^{3+} and Ga^{3+} ions.

The aim of the present work is to study the interplay between the transport and the magnetic properties of the pure $\lambda-(BETS)_2FeCl_4$ phase ($x = 1$) and, in the light of the discussion above, to determine whether its ground state is AF or not. At high temperature the spins of the Fe^{3+} ions are paramagnetic while the 2D conduction carriers are in a metallic paramagnetic state. On the one hand, from magnetoresistive data [16a], the insulating ground state was thought to result from the condensation of the 2D conduction carriers into a SDW induced by an AF ordering of the Fe^{3+} localised spins. On the other hand, whereas ESR measurements performed on "powder" (polycrystalline) sample have also detected AF interactions in the metallic state, they rather may suggest a non magnetic ground state [9].

In order to explore in more details the previously published temperature-magnetic field phase diagram [16a], both magnetization (static and dynamic) and magnetoresistive measurements in steady fields are reported. An interpretation based upon a generalized Kondo lattice is consistent with the experimental data: for applied magnetic fields greater than 10 T, the field-restored highly conductive state (FRHCS) results from a field-induced (possibly not full) oriented paramagnetic ordering of the Fe^{3+} and (possibly) itinerant spins along the field direction.

2 Experimental

Neutral bis(ethylenedithio)tetraselenafulvalene (BETS) was prepared according to the previously reported method [4]. Crystals of charge transfer salts with the $(FeCl_4)^-$ anion having the $(BETS)_2(FeCl_4)$ stoichiometry were prepared by electrochemical oxidation of BETS (6 mg) in 20 ml of chorobenzene/ethanol (90/10) containing $(Et_4N)(FeCl_4)$ (40 mg). A mixture of plate-shaped and needle-shaped phases, designated $\kappa-(BETS)_2FeCl_4$ and $\lambda-(BETS)_2FeCl_4$ respectively, is obtained when the electrolysis current is kept constant at 0.5–0.6 μA. When the potential at the electrodes is kept constant at either 3.7 V or 3.3 V, the dominant species collected at the anode is the plate-shaped $\kappa-$ or the needle-shaped $\lambda-(BETS)_2FeCl_4$ phase, respectively.

Crystallographic data for both phases were obtained with a four-circle diffractometer and a low-temperature imaging plate X-ray system equipped with a closed-cycle helium refrigerator. These previously reported [10] studies have shown that the plate-shaped and needle-shaped phases possess $\kappa-$ and $\lambda-$type structures, respectively. $\kappa-(BETS)_2FeCl_4$ has an orthorhombic lattice with space group Pnma, whereas $\lambda-(BETS)_2FeCl_4$ belongs to triclinic system with space group $P\bar{1}$. Oscillation photographs were taken at temperatures varying down to 7 K. The graphite monochromatized MoKα radiation ($\lambda = 0.7107$ Å) was used.

After a slow cooling of the needle-like samples, transverse magnetoresistive measurements were carried out during the slowly decreasing part (1.2 s) of pulsed fields B as large as 37 T. The data were classically recorded with an alternating (50 kHz) current I (77 μA in the metallic ($T > 8.5$ K) and 100 nA in the dielectric ($T < 8.5$ K) states). The current was flowing either along the best conduction c-axis of the needle or along the b'-axis, where b' is $\perp$ to the c-axis in the bc-plane. Four probe measurements were realized through annealed gold wires (17.5 μm in diameter) glued by graphite paste on four pre-evaporated gold contacts upon the sample. In order to avoid resistivity cracks induced by thermal shrinks of the paste, a pressed-contact system based on platinum wires (20 μm in diameter) bended on these gold contacts was also used. A sample holder allowing rotation of the needle around its c-axis yields transverse magnetoresistance data for discrete values of the angle θ between the magnetic field direction and a', with $a' \perp c$-axis in the ac-plane.

Transverse magnetoresistance measurements were also carried out in steady fields delivered by a superconducting 15 T coil: in this configuration, the needle was rigidly sticked to four platinum wires with very fine gold paste

and located close to a microcantilever used for magnetization measurements. This microcantilever has been produced by a microlithographic technique from single crystal silicon [17], and allows for sensitive detection of static magnetic moment μ through force $F = \mu \times \nabla B$ and/or torque τ measurements. Measurements were performed on a sample consisting of two needle-like thin single crystals, aligned with needles parallel to each other but randomly oriented in the transverse direction. They were fixed with vacuum grease upon the upper sensitive part of the cantilever. A magnetic field gradient ∇B was created by some axial displacement of the device apart from the field center. Since the two crystals were not oriented with respect to the *ac*-conducting plane, the recorded capacitance change of the magnetometer has anisotropic and isotropic components, providing both torque and force signals in fields applied perpendicularly to the needle *c*-axis. Both magnetic field and temperature sweeps were recorded and the capacitance signal of the empty magnetometer was substracted from the data. It is worth noting that this signal was almost temperature and field independent in temperatures lower than 18 K and in fields of up to 14 T.

SQUID measurements were performed with a Quantum Design magnetometer firstly by measuring the static magnetization at fixed temperatures and secondly by sweeping the temperature in the range 2-300 K in magnetic fields of up to 7 T. The field was applied along two directions, either roughly parallel or perpendicular to the *c*-axis of the needle-like crystals (1.49 mg and 0.63 mg, respectively) sealed together in a thin quartz capillary (0.7 mm in diameter). In both cases the very weak diamagnetic contribution of the sample holder was not subtracted from the recorded experimental data.

Two single crystals ($2\times0.2\times0.1\,\mathrm{mm}^3$) of $(BETS)_2FeCl_4$ were studied by Electron Spin Resonance (ESR) and Antiferromagnetic Resonance (AFMR) techniques using a Bruker ESP-300E spectrometer equiped with a cryostat ESR 900 (3.7 K - 300 K) from Oxford Instruments. X-ray refinements have certified that both crystals crystallize within the λ phase [18].

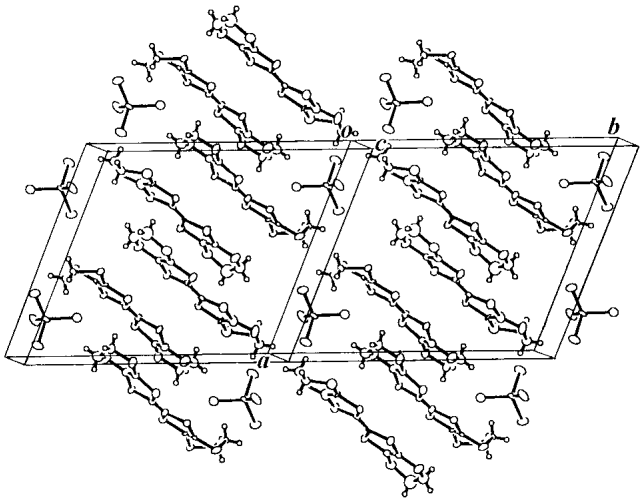

Fig. 1. Crystal structure of $\lambda-(BETS)_2FeCl_4$.

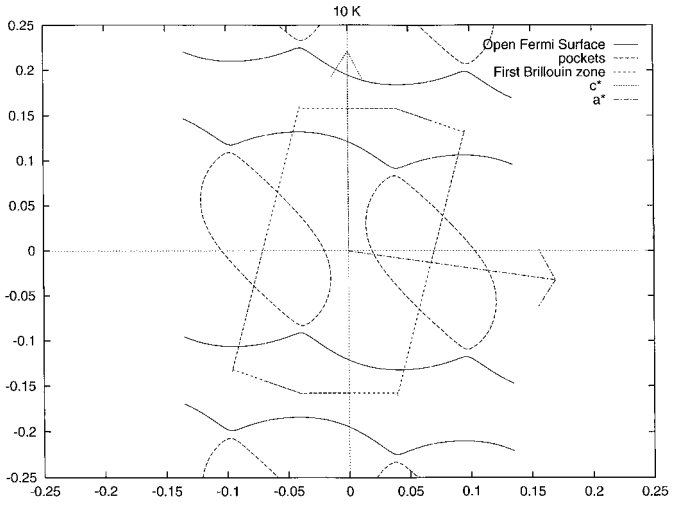

Fig. 2. Fermi surface of $\lambda-(BETS)_2FeCl_4$ at 10 K.

3 Results

3.1 Crystal and electronic band structures

As previously described [10], the BETS molecules are stacked along the *a*-axis (Fig. 1). The structural arrangement may be described as two-dimensional sheets of BETS molecules parallel to the *ac* plane with linear columns of $FeCl_4$, intercalated between these sheets and yielding several Cl-S (Se) interatomic distances shorter than the corresponding sum of the van der Waals radii. In this work, the lattice constants were determined again at 298 K and 10 K, and are as follows: at 298 K, $a = 16.164(3)$, $b = 18.538(3)$, $c = 6.592(4)$ Å, $\alpha = 98.40(1)°$, $\beta = 96.69(1)°$, $\gamma = 112.52(1)°$; at 10 K, $a = 15.880(6)$, $b = 18.378(3)$, $c = 6.529(4)$ Å, $\alpha = 98.66(5)°$, $\beta = 95.830(4)°$, $\gamma = 112.13(2)°$. The direct distances between Fe^{3+} nearest neighbours along the *a*-direction in the anion layer are equal to 10.1 Å within each unit cell and to 8.8 Å between neighbouring unit cells.

Extended Hückel tight-binding band structure calculations were carried out for the structure determined at 10 K. The intermolecular overlap integrals of the highest occupied molecular orbitals (HOMO) differ from those published in reference [10], because they were calculated by a slightly modified Wolfsberg-Helmholz formula [19] using single-zeta Slater-type orbitals on the C, S and Se atoms. These calculations yield i) a corrugated extended Fermi sheet of electron character and ii) a hole-like two-dimensional (2D) closed Fermi surface, the area of which being equal to 18% of the first Brillouin zone area (Fig. 2).

3.2 Magnetoresistive experiments

The temperature dependence of the resistivity of $\lambda-(BETS)_2FeCl_4$ at ambient pressure is known to display [7]: i) a resistivity maximum around 90 K very

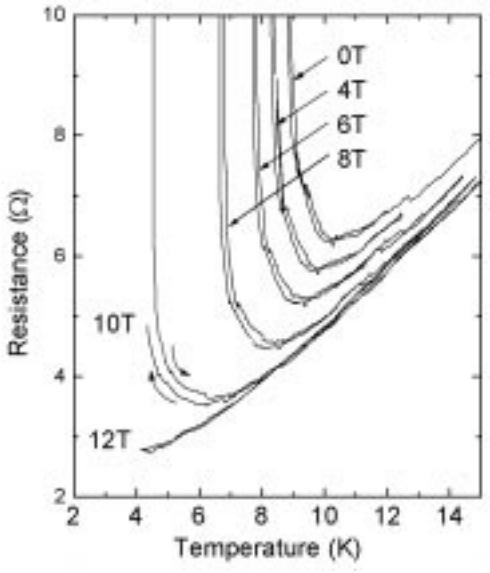

Fig. 3. Temperature-dependence of the resistance in different static magnetic fields $B \perp I \parallel c$. Arrows indicate the different directions of the temperature sweeps and reveal the M-I transition hysteresis.

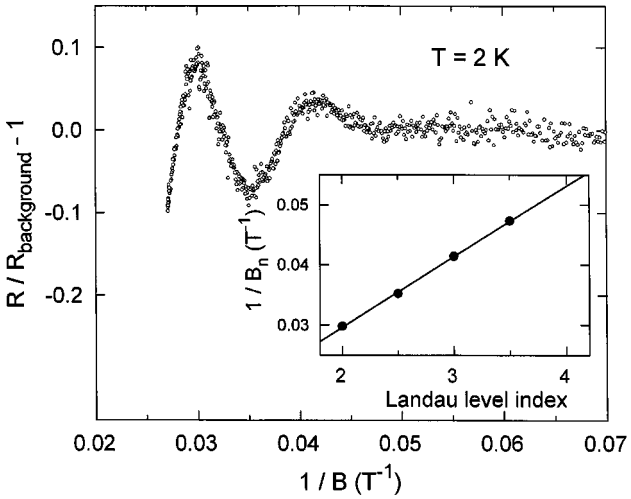

Fig. 4. Shubnikov-de Haas like oscillations of the magnetoresistance recorded at 2 K with $I \perp c$ and $\theta = (\mathbf{B}, a') = 130°$ (see text).

similar to the one observed in the temperature dependence of the resistivity of many $\kappa-(\text{BEDT-TTF})_2\text{X}$ salts, ii) a resistivity minimum at 10 K and iii) a sharp metal-insulator (M-I) transition below 9 K. Under applied magnetic field, the temperature of the resistivity minimum decreases as the field increases, as displayed in Figure 3. This field-induced suppression of the M-I transition observed in the temperature dependence of the resistance is in agreement with the huge negative magnetoresistance previously noticed in pulsed fields experiments [16a]. It is worth to note that this field-induced restoration of a highly conducting state displays a hysteresis which increases as the magnetic field increases. This hysteresis is visible even if $B = 0$, which constitutes a strong evidence of the first order character of the M-I transition. This transition cannot be thus understood only within the framework of a progressive gap opening in the one-particle excitation spectrum which characterizes the condensation of spin or charge density wave instabilities in low dimensional electron gas.

Above 12 T, the resistance, measured under transverse applied magnetic fields at low temperature, is known to follow almost quadratic power laws $R = R_0 + CB^\alpha$, where $\alpha = 1.85$ and C exhibits minimum and relative maximum value for $\theta = 0°$ ($B \parallel a'$) and 110° ($B \parallel b'$), respectively [16a]. In contrast to that, the magnetoresistance recorded at $T = 2$ K, $\theta = 130°$ and for $I \perp c$, exhibits weak but significant quantum oscillations periodic in $1/B$ (Fig. 4). The field direction in this figure corresponds to the direction of the applied field for which the angular dependence of the semiclassical magnetoresistance is maximum [16b]. The inset of Figure 4 shows that i) the maximum of the oscillation which occurs at $B_n = 33$ T is related to the Landau level $n = 2$ and ii) the fundamental frequency of the Shubnikov-de Haas like oscillations is (85 ± 5) T. This frequency corresponds to a cross-section area of closed orbits equals to about 2% of the first Brillouin zone area, which is obviously one order of magnitude less than predicted by band structure calculations [10].

3.3 Magnetic measurements

3.3.1 Static susceptibility on polycrystalline sample

In the metallic state ($T \geq 9$ K), the magnetic moment M measured in field applied parallel to the c-axis, displays good linearity at low field, as shown in Figure 5. At higher fields, begins to appear a pronounced downwards curvature which is the signature of field-induced alignment of the magnetic moments.

Figure 6 displays the field dependence of the magnetic moment recorded for applied fields $\parallel$ to the c-axis and at low temperatures ($T < 9$ K) in the insulating state. Whereas the above-mentioned saturating trend begins to occur above 6 T, the magnetic moment is far from reaching the saturation value of the iron momentum even at magnetic field as high as 7 T. A departure from the linear magnetization appears at low field: the lower the temperature, the more pronounced the non-linearity. This field dependence of the magnetization can be splitted up into three parts: a very low field ($B < 0.5$ T, *cf.* inset of Fig. 6) and a high field (3 T $< B <$ 6 T) parts in which the magnetization is proportional to the magnetic field, and a non-linear intermediate behaviour which is reminiscent of a spin-flop transition [20] occuring in the insulating state as discussed later. If we choose the midpoint of this phase transition as the inflexion point in the curves, an almost temperature insensitive value of about 1.1 T is obtained. It is worth to stress upon that no hysteresis is observed in this non-linear behaviour. On the other hand, no deviation from linearity is observed for fields applied perpendicularly to the needles axis.

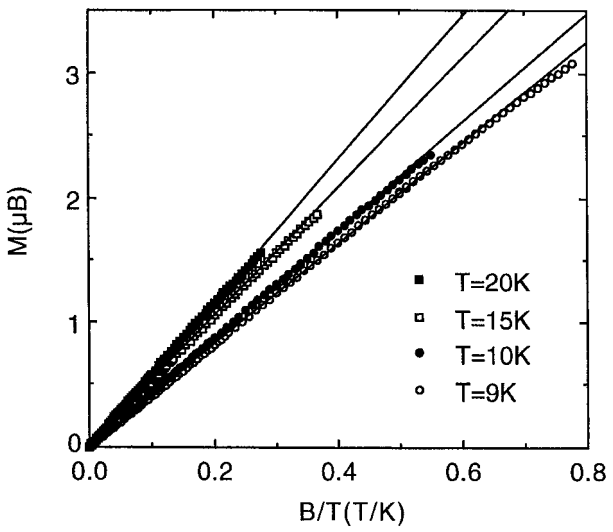

Fig. 5. Plot of the magnetic moment *versus* magnetic field over temperature, in the temperature range 9 to 20 K. The magnetic field is parallel to the c-axis. Magnetic moment is expressed in μ_B per Fe^{3+} units. Solid lines are best linear fits at low fields.

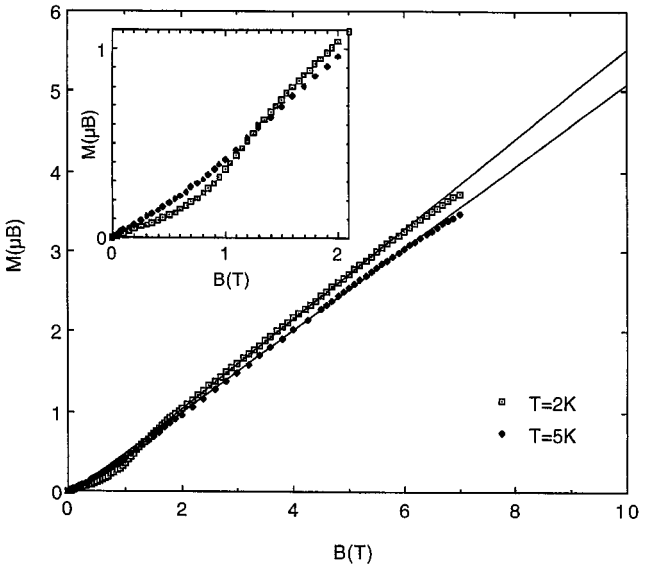

Fig. 6. Magnetic field dependence of the magnetic moment at $T = 5$ and 2 K. Eye-guide solid lines show linear recovery at intermediate field (3 T $< B <$ 6 T). (Inset: low field non-linear magnetic moment at $T = 5$ and 2 K).

We have verified that the temperature dependence of the inverse susceptibility B/M is in agreement with the Curie-Weiss law $C/(T - \theta)$ in the metallic state. This confirms the occurrence of AF interactions as previously stated through the ESR measurements performed on the same polycrystalline sample [10]. Using the stoichiometric ratio of one $FeCl_4$ per formula unit and the value $\theta = -15$ K derived from the spin susceptibility only [10], the deduced value of the Curie constant $C = N\mu^2/(3k_B)$ yields an effective magnetic moment μ of 5.83 Bohr magneton μ_B. This is very close to the value (5.92 μ_B) of the magnetic moment of Fe^{3+} in its high spin state ($S = 5/2$ and $L = 0$). This means that the measured magnetization arises mainly from the localised spins along the chains and not from the conduction electrons of the (BETS) donors in the two dimensional sheets. This point can also be inferred from the value of the susceptibility $\chi = 10^{-7}$ emu/Oe measured at room temperature. This corresponds to a molar susceptibility of about 10^{-1} which is two orders of magnitude greater than those currently measured in pure organic compounds. Using $\theta = -15$ K and $S = 5/2$ leads to an exchange parameter J_0 between the Fe^{3+} spins $J_0 = 0.2$ meV.

Figures 7 and 8 display the temperature dependence of the static susceptibility χ below 15 K, for field roughly

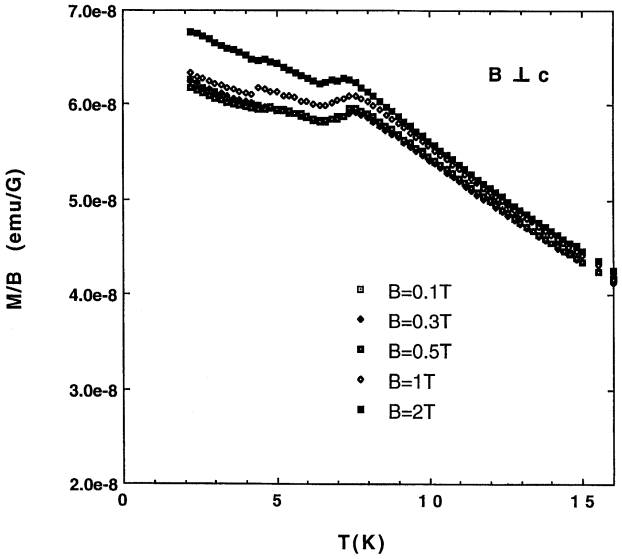

Fig. 7. Low temperature dependence of the static susceptibility with $B \perp c$ axis of the needles.

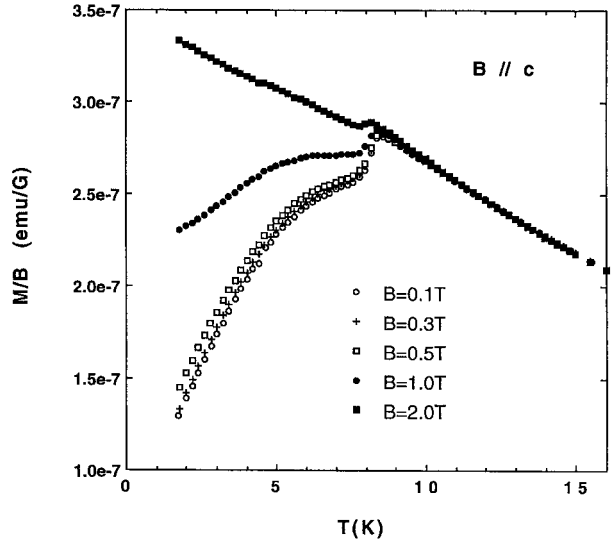

Fig. 8. Low temperature dependence of the static susceptibility with $B \parallel c$ axis of the needles.

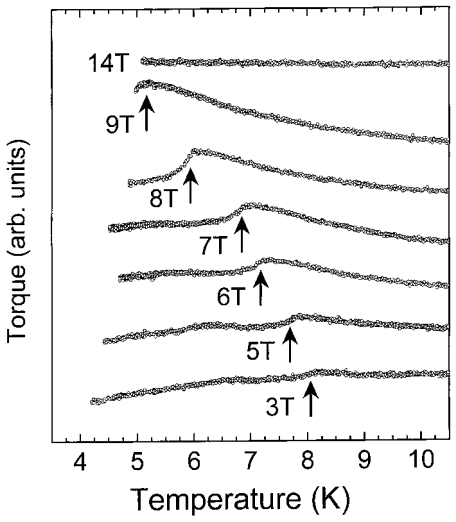

Fig. 9. Low temperature dependence of the torque signal τ derived from cantilever measurements in different magnetic fields. Arrows depict the M-I phase transition.

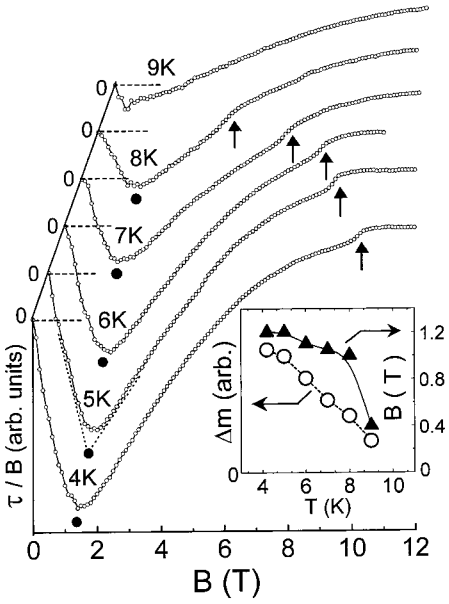

Fig. 10. Magnetic field dependence of the torque signal τ over the field at different temperatures. Arrows point on the M-I phase transition. Inset: temperature dependences i) of the magnetization jump (○) at the M-I phase transition and ii) of the field value (▲) at which occur the recorded (●) minima of τ/B.

applied $\perp$ and $\parallel$ to the c-axis, respectively. As previously published [20], this behaviour is typical of AF ordering of the spins along an easy axis of magnetization close to the c-axis. For field applied $\perp$ to the c-axis, the χ values should be regarded as an average since the field is statistically applied perpendicularly to the ac and bc planes of the polycrystalline sample.

In low fields ($B < 2$ T) applied along the c-direction, it is worth to comment on the unusual decreasing mode of the susceptibility below 8.5 K. As the temperature decreases, a weak decrease first sets up with a positive curvature, but is followed below 7 K by a second decrease with a negative curvature. Such departure from the monotonous mean field decrease of the susceptibility may rely on the low dimensionality of the compound or on the first order character of the phase transition (see discussion).

3.3.2 Cantilever results

The temperature dependence of the torque τ displayed in Figure 9 has been derived from the capacitance changes ΔC (through $\Delta C \sim \mu \times B$) recorded at low temperature in different magnetic fields. In fields of up to 9 T and below 9 K, a more or less prominent hump, depicted by solid arrows in Figure 9, is observed. This feature increases in magnitude and shifts towards low temperature with increasing field. Its location is in very good agreement with the M-I phase transition obtained by magnetoresistive measurements either in pulsed field [16] or in steady field (see Fig. 3). The torque units are unquantified due to the lack of precise knowledge of the angle between the applied field and the net magnetization vector, but in each trace, the moment change at the transition is of the order of 5×10^{-11} Am^2, or 5×10^{-9} emu.

Similarily, Figure 10 displays perpendicular magnetization (τ/B) data which have been also derived from

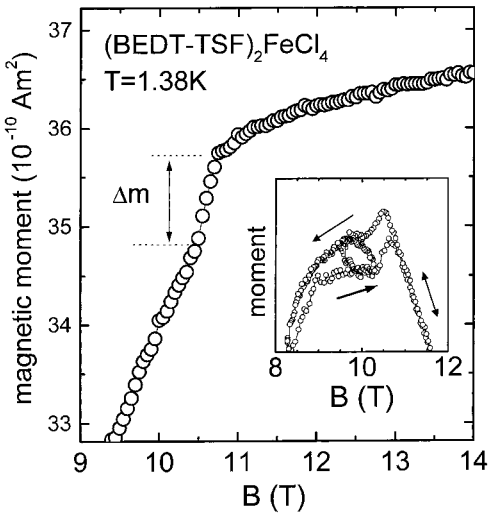

Fig. 11. Blow-up of the magnetic field dependence of the magnetic moment derived from capacitance measurements at $T = 1.38$ K. Inset: hysteresis and hysteretic loop recorded in the dielectric state.

the magnetic field dependence of the capacitance changes ΔC. Jumps depicted by arrows sign again the previously mentioned M-I phase transition. As observed in Figure 9, these jumps are more clearly seen at lower temperature, as confirmed by the positive and hysteretic paramagnetic-tending jump Δm in the magnetic moment plotted in Figure 11. Coming back to Figure 10, black dots assign magnetic anomalies which occur at fields comprised between 1.0 and 1.2 T, *i.e.* very close to the field value of

1.1 T assigned to the inflexion point obtained in the SQUID measurements. It is worth to note that the low field decrease of τ/B does not reflect a diamagnetic response of the measurements. Indeed, torque does not measure the moment parallel to the applied field, but the resultant component of the magnetization normal to it. More precisely, keeping in mind the c-axis is the axis about which torque is measured, the torque is sensitive to the difference between the moments along the two perpendicular axes.

3.3.3 ESR and AFR on single crystal

As above mentioned, previous experiments on a polycrystalline sample have been already published [10]. A single ESR line was reported. At room temperature, the authors obtain $g \sim 2.05$, a peak-to-peak linewidth $\Delta H_{\rm pp} \sim 220$ G. When decreasing the temperature, both the g factor and linewidth increase while the spin susceptibility follows a Curie-Weiss dependence ($\theta \sim -15$ K). To deepen this analysis we have undertaken measurements on single crystal.

At room temperature, a large anisotropy of both the linewidth and the g factor is observed. In particular, the linewidth goes to a deep minimum ($\Delta H_{\rm pp} \sim 180$ G) with $g \sim 2.05$ when the magnetic field is aligned in an undefine direction (labelled u in the following) in the plane perpendicular to the c-axis. We obtain $\Delta H_{\rm pp} \sim 700$ G, and $g \sim 2.22$ when the field is along c. Due to the small sample size, a quantitative study of this anisotropy has been impossible. It is worthwhile to notice that our results are in agreement with the previous work since the data collected from a "powder experiment" are dominated by the orientations corresponding to the smallest linewidths. Moreover, it should be noted that similar values of the linewidth (400 G) and g factor (2.017) have been recently reported in $(BET)_2FeCl_4$ which incorporates the same paramagnetic anion [21].

We have first studied the temperature dependence of the ESR signal with the magnetic field along the u-direction. Results are reported in the lower part of Figures 12 and 13 and in Figure 14. The linewidth increases when cooling while the g factor goes to a weak maximum around 50 K. The spin susceptibility first follows a Curie-Weiss dependence with $\theta \sim -15$ K, in agreement with [10]. Below 10 K we observe a sharp decrease of the susceptibility in agreement with previous static results. This anomaly should be related to the occurrence of the already mentioned phase transition at $T_{\rm c} \sim 8$ K. We shall therefore discuss separately the results below this temperature. Note that the line-shape is no longer Lorenztian below 100 K. The anisotropy A/B of the line increases under cooling down to 10 K when the symmetry of the line is progressively restored (see inset of Fig. 14). Such a behaviour was already observed in the previous experiment [10]. The effect is simply more pronounced in our case.

In order to characterize the paramagnetic phase in more details we have tried to obtain further results in the case where the magnetic field is oriented along the c-axis.

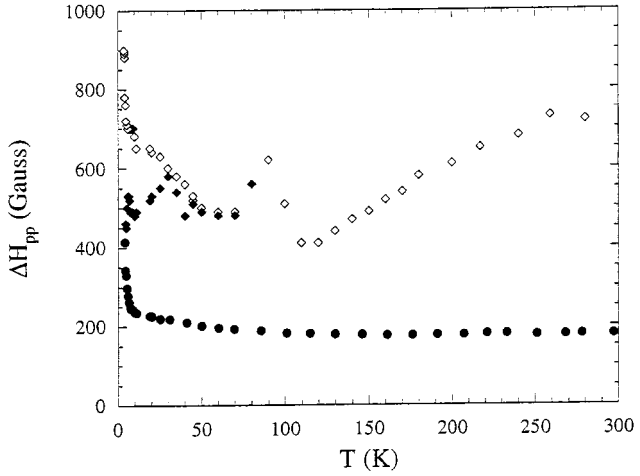

Fig. 12. Temperature dependence of the ESR linewidth for field applied either along u (lower part of the figure) or c-directions (upper part of the figure) of single crystal of λ−$(BETS)_2FeCl_4$.

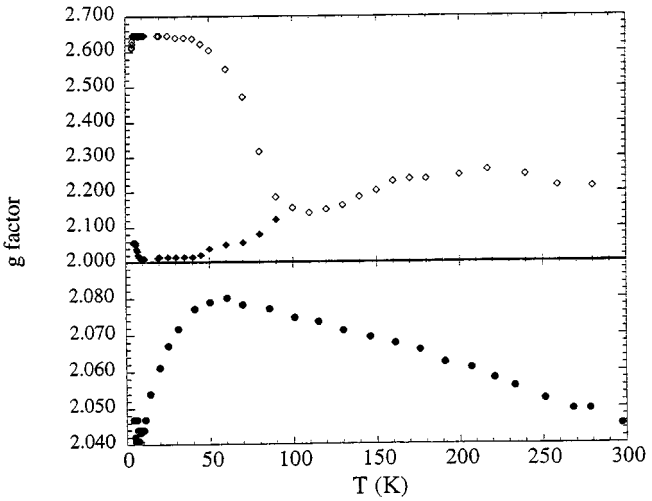

Fig. 13. Temperature dependence of the g factor for field applied either along u (lower panel of the figure) or c-directions (upper panel of the figure) of single crystal of λ−$(BETS)_2FeCl_4$.

Because of the larger linewidth, the data are less accurate but provide complementary informations. The data are displayed in the upper part of Figures 12 and 13 and in Figure 14. The linewidth decreases down to 100 K where a more complex behaviour is found. As a matter of fact, the signal splits into two lines with different g factors. This splitting which may be already present at 100 K becomes clearly visible below 70 K in particular when the g factor is considered (see Fig. 13). It should be noticed that the lower ESR line with $g \approx 2.0$ has a linewidth and an intensity much lower than the upper one with $g = 2.6$. Within the experimental accuracy, the temperature dependence of the spin susceptibility is orientation independent in the paramagnetic - metallic state (Fig. 14).

Let us now discuss the data recorded at low temperature (below 8 K). Figure 15a shows a rotation pattern

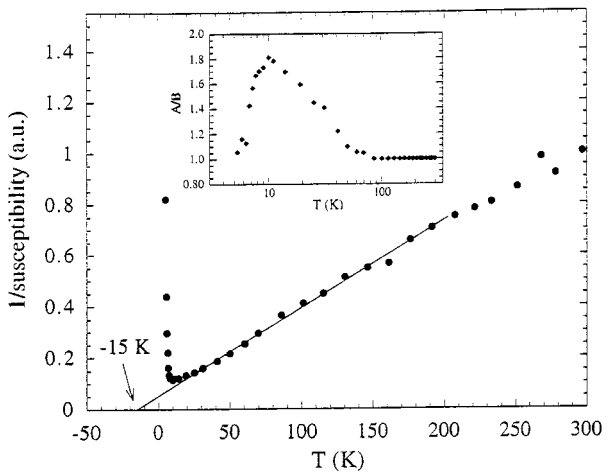

Fig. 14. Plot of the inverse spin susceptibility of a single crystal of λ−(BETS)$_2$FeCl$_4$, for field applied along the c- or u-directions. Inset: temperature dependence of the anisotropy ratio A/B of the ESR resonant line.

of the resonance field at 6.8 K (*i.e.* sligthly below T_c). In this experiment, the magnetic field is rotated in a plane roughly containing both c and u directions (in Fig. 15a and 15b, θ is the angle between the field direction and c). Around the c-direction, the ESR line with $g \approx 2$ is not displayed since its intensity is very weak compared with the others. Far from the c-direction, a single line, reminiscent of the ESR signal, is observed. However, another resonance is found close to the c-direction at higher field, showing a rotation pattern characteristic of AF resonance [22]. The extremum of this "bubble"-like pattern is found at about 25° from c. A similar rotation pattern at 3.7 K (*i.e.* far below the phase transition), is displayed in Figure 15b. Only the antiferromagnetic signal is observed for fields applied along directions close to the c-axis. The slightly asymmetric shape of the bubble indicates that the rotation plane is not simple although the easy axis of magnetization should be close to c. Moreover, the rotation pattern should remain close to an easy intermediate pattern [22] with a spin-flop field of about 1.1 T. This result definitely confirms the AF nature of the low temperature phase and is in agreement with the above reported static measurements (Figs. 7, 8 and 10). Finally, the temperature dependence of the resonance fields is displayed in Figure 15c (in the field orientation shown by an arrow in Figs. 15a and 15b). The results are in agreement with the theory: the field corresponding to the lower resonance goes to zero as the temperature increases towards T_N, whereas the upper mode remains weakly temperature dependent [23].

4 Discussion and interpretation

Let us discuss the nature of the ground state of λ−(BETS)$_2$FeCl$_4$ and the specific details of its (T−B) phase diagram, including the non-linear magnetization regime.

As shown in Figures 7 and 8, an anisotropic field dependent magnetic susceptibility is found below 1 T. In addition, antiferromagnetic resonance is observed below 8 K. Both data firmly establish the existence of a long-range AF order at low temperature. The "bubble-like" pattern shown in Figures 15a and b indicates a spin-flop field of about 1.1 T with an easy axis close to c, correlated with the minimum recorded in the torque measurements (Fig. 10) and in perfect agreement with the static measurements displayed in Figure 6. In this latter case, the effect of the first order spin-flop transition is smeared out by the average over the polycrystalline sample. It is remarkable that a similar value of the spin-flop field is found in many organic compounds [24], suggesting a common origin of the magnetic anisotropy (dipolar interactions or spin-orbit coupling). Similar first order non linearities occur also between the low field dimerized (D) and the high field incommensurate (I) subphases of the spin-Peierls (SP) ground state of $S = 1/2$ Heisenberg-XY spin chains, such as TTF-BDT(Cu) [25]. Despite this similarity, our results definitely establish the AF nature of the ground state and are quite conventional in weakly anisotropic Heisenberg AF materials like other organic salts [26].

However, a more complex behaviour is found in the present case. First, the AF rotation pattern at 6.8 K (Fig. 15a) shows an extra low field resonance. Furthermore, the temperature dependence of the magnetic susceptibility along c (Fig. 8) which gives an estimation of the so-called $\chi_{\parallel}$ component (when the magnetic field is parallel to the magnetic moments) has a non conventional temperature dependence. Although the origin of such a distinctive behaviour is not clear, one may argue that the present material involves two kind of spins (conduction electrons of the organic molecules and localized Fe^{3+} spins). As mentioned previously, the conduction electrons do not contribute significantly to the susceptibility in the paramagnetic (conducting) state. However, they may become important in the insulating AF state. This unusual interplay between the two spin species may also be at the origin of the first order character of the para-AF phase transition.

Gathering all the present magnetoresistive and magnetization data yields the phase diagram of Figure 16. A spin-flop line separates the uniaxial AF ground state from a canted antiferromagnetic (CAF) one. Within a molecular field approximation, the "spin-flop" field B_{sf} (≈ 1 T) is the geometric mean $B_{sf}^2 = B_a B_c$, where B_a and B_c denote respectively the anisotropy field and the field (≈ 10 T) of the transition from the CAF to the oriented paramagnetic state. Using $B_c = 2B_{ex} - B_a$, we derive both B_a (≈ 0.1 T) and the exchange field B_{ex} (≈ 5 T). Thus we get $B_a \ll B_{ex}$, in agreement with the conditions required to observe "spin-flop" rather the metamagnetic transitions observed in $FeCl_2$ [27] or DAG, an Ising AF [28]. Besides this first order spin-flop line, one may notice the unusual shape of the paramagnetic-antiferromagnetic curve. Indeed the transition temperature significantly decreases when the magnetic field is applied: usually, quadratic weak

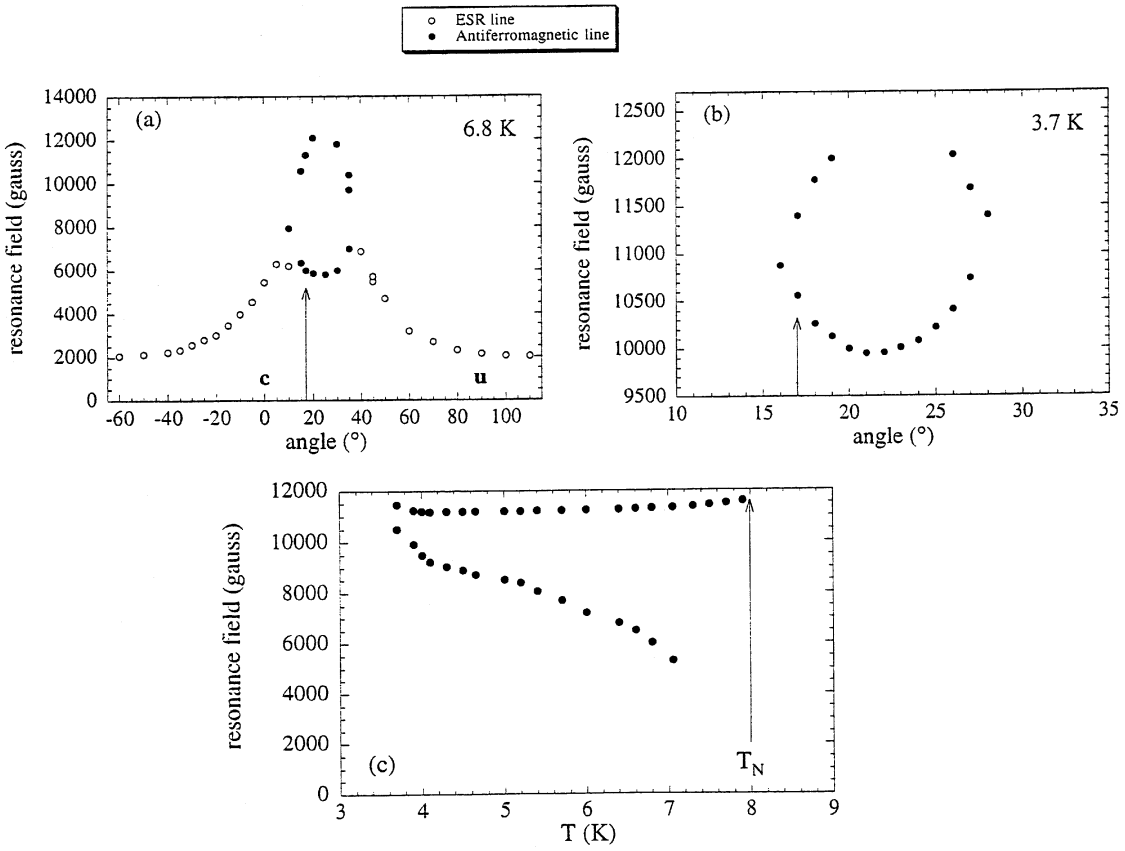

Fig. 15. Angle dependences of the electron spin and AF resonant fields at 6.8 K (a) and 3.7 K (b). Characteristic AF "bubble"-like rotation patterns are displayed in Figures 15a and 15b. Arrow indicates orientation of the applied field for which the temperature dependence of the resonance fields is plotted in Figure 15c.

field dependences are found in other materials [29], including Peierls [30] and spin-Peierls [31] compounds. Instead of that, a decrease either linear or with a positive curvature of T_N is observed at low field, within the uncertainty of our measurements. Moreover, a crossover is observed around 4 T and the AF order is even more strongly affected by the magnetic field above this point. Finally an almost saturated paramagnetic order is stabilized down to very low temperature above 11 T. There is no apparent discontinuity between the low field-high temperature paramagnetic state and the high field-low temperature oriented paramagnetic state. Nevertheless, the very weak $S\mathrm{d}H$ oscillation frequency measured (above 10 T) in that state suggests that its corresponding FS should be different from the one calculated from the 10 K crystalline structure in zero field (Fig. 2). This point will be cleared up in the following interpretation.

This peculiar phase diagram topology may be related to the first order character of the phase transition. In this context, it is clearly relevant to discuss the characteristics of the AF ordering in terms of a system of coupled conduction and localized electrons. This is the purpose of the following part of the paper.

The experimental results demonstrate that, the magnetic susceptibility is dominated by the contributions of the $S = 5/2$ Fe^{3+} ions which are far apart (6.5 Å in the c chain direction and even greater in the a-direction). Moreover, since the two magnetic ions per unit cell are separated by the Cl^- ions, a large direct exchange seems unlikely. The dominant interaction is likely to be a double exchange between the iron moments *via* the Cl^- tetrahedra and the spins of the conduction electrons on the overlapping BETS orbitals. This experimental situation seems to be well accounted for by Figure 17 in which the spins on the iron atoms S_a and S_b are drawn i) for the special case of a simple periodic order from unit cell to unit cell and ii) antiparallel to emphasize that in general they need not be parallel. As they interact indirectly *via* the spins s of the conduction plane they may be at an arbitrary angle. The itinerant spins s are drawn in a SDW and insulating ground state, and antiparallel to the localised moment S to emphasize that there is an antiferromagnetic exchange. Experimentally, we know that the spins are not collinear with the crystal axes, and we shall hypothesize, based on calculation, that they are not collinear with one another. In practice we will consider more general order with non collinear order from unit cell to unit cell, though for numerical minimization we will restrict ourselves to spins a and b parallel. We shall take the simplest description of the electronic properties compatible with this picture by

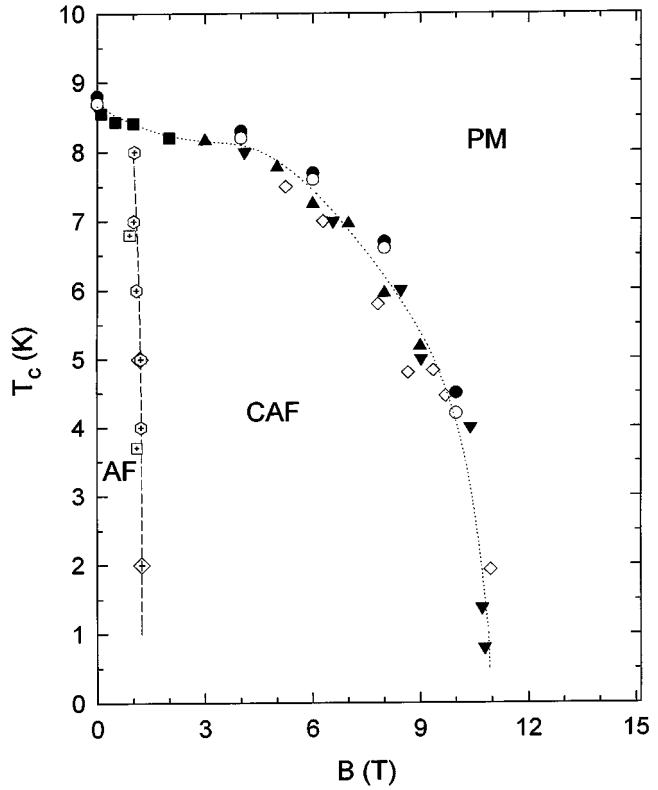

Fig. 16. $T-B$ phase diagram of $\lambda-(BETS)_2FeCl_4$. All the points were collected from the different experiments reported here. The dotted line corresponds to the "spin-flop" transition between uniaxial (AF) and canted (CAF) antiferromagnetic states.

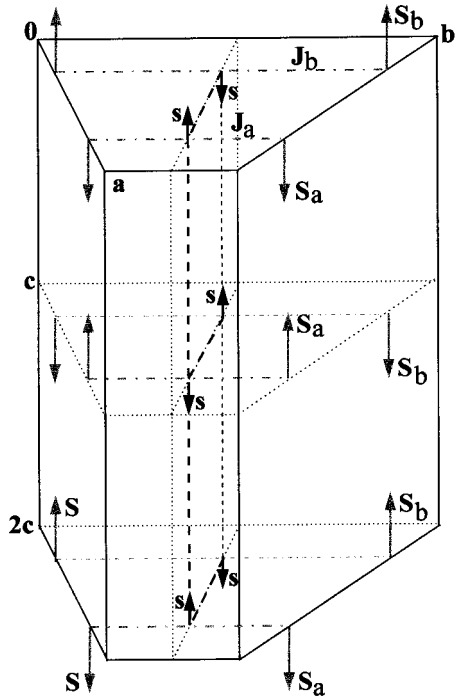

Fig. 17. Schematic diagram showing the indirect exchange couplings J_a and J_b between the spin s of the conduction electrons and the Fe^{3+} spins S_a and S_b. The Fe^{3+} are respectively localised along two independent 1D stacks located at two different distances from the 2D ac conducting sheet (see text). The structure is drawn for the special case of a commensurate ordering vector which, unlike the general case considered, is collinear.

writing a generalized Kondo lattice model [32] with four bands and two magnetic ions as described by the following Hamiltonian

$$H = \sum_{i,j} \sum_{\sigma_z=\pm 1} t_{i,j}(c^{\dagger}_{i,\sigma_z} c_{j,\sigma_z} + hc) + U \sum_i n_{i\uparrow} n_{i\downarrow} + \sum_{i_a,i} J_a(i_a,i) S_{i_a} \sigma_i + \sum_{i_b,i} J_b(i_b,i) S_{i_b} \sigma_i + g_{Fe^{3+}} \mu_B \sum_{i_a} S_{i_a} B + g_{Fe^{3+}} \mu_B \sum_{i_b} S_{i_b} B + g \mu_B \sum_i \sigma_i B. \quad (1)$$

Here i_a and i_b define the set of two Fe^{3+} ions running along two chains $\parallel$ to c-axis (Fig. 17) and the summations over the 4 inequivalent bands i of each unit cell are over the set of all HOMO orbitals. μ_B is the Bohr magneton. The $t_{i,j}$'s are taken from the extended Hückel calculations derived at 10 K which — without any contribution of the magnetic coupling — yield the Fermi surface of Figure 2. In the above Hamiltonian, the coupling in finite magnetic field B is included *via* coupling to the spins of the Fe^{3+} moments and to those of the conduction electrons only, neglecting any coupling to the orbital motion *via* a Peierls substitution. The components σ_i^j of the spin operators σ_i for the HOMO orbital i of the conduction electrons are defined as:

$$\sigma_i^j \equiv \sum_{\mu,\nu} c^{+}_{i,\mu} \sigma^j_{\mu,\nu} \; c_{i,\nu} \quad (2)$$

$\sigma^j_{\mu,\nu}$ are the Pauli matrices ($j = 1,2,3$) g_{Fe} and g are the Landé factors of the Fe^{3+} ions and the electrons in the HOMO orbitals, respectively. U is an assumed intramolecular Coulomb interaction. For the sake of simplicity, anisotropy in the g tensor, *i.e.* crystal field effects on the Fe^{3+} ions are neglected. Since a spin-flop rather than a metamagnetic transition is observed, the magnetic anisotropy energy is supposed to be weak compared to the exchange energy and is thus also neglected. Since the spin S is large and there are at most two partially filled bands, in Kondo language we are in an under-screened situation. We expect thus the ground state to be dominated by RKKY-type exchange interactions that we shall treat firstly perturbatively. To lowest order, the exchange is just the RKKY interaction between the spins localised along the two chains a and b, *via* the conduction band. This is related to, although it is not exactly the same as, the magnetic susceptibility of the conduction bands and thus reflects the geometry of the FS. In a second step, we shall include the effects of the magnetic order interacting back on the conduction band. In a third step will be shortly derived an argument showing how the coupling between

the localised spins *via* the itinerant ones yields a first order phase transition in the (T, B) phase diagram instead of an expected second order one as should be the case for independent spins populations.

More precisely the RKKY exchange interactions $J^{\rm aa}(q)$, $J^{\rm bb}(q)$ and $J^{\rm ab}(q)$ are given by

$$\begin{aligned} J^{\rm aa}(q) &= \sum_{\alpha,\beta} f^{\rm aa}_{\alpha,\beta}\chi_{\alpha,\beta} \\ J^{\rm bb}(q) &= \sum_{\alpha,\beta} f^{\rm bb}_{\alpha,\beta}\chi_{\alpha,\beta} \\ J^{\rm ab}(q) &= \sum_{\alpha,\beta} f^{\rm ab}_{\alpha,\beta}\chi_{\alpha,\beta} \end{aligned} \tag{3}$$

where

$$\chi_{\alpha,\beta}(\mathbf{Q}) = -\frac{2}{\nu}\int \frac{n(\varepsilon^{\alpha}_{k+\mathbf{Q}}) - n(\varepsilon^{\beta}_{k})}{\varepsilon^{\alpha}_{k+\mathbf{Q}} - \varepsilon^{\beta}_{k}}{\rm d}k, \tag{4}$$

$n(\varepsilon)$ is the Fermi-Dirac distribution function and ε^{α}_{k} are the dispersion of the bands α. The $f^{\rm aa}$, $f^{\rm bb}$ and $f^{\rm ab}$ are calculated from the $J_{\rm a}(i_{\rm a}, i)$ the $J_{\rm b}(i_{\rm b}, i)$ of equation (1) and from the matrix diagonalising the conduction band, indexed by α and β:

$$\begin{aligned} W^{p}_{\alpha,\alpha} &= \sum_{i} J_p(i_p, i)|\langle i|\alpha\rangle|^2 \\ W^{p}_{\alpha,\beta} &= \sum_{i} J_p(i_p, i)\langle\beta|i\rangle\langle i|)\alpha\rangle \\ f^{p,q}_{\alpha,\beta} &= (W^{q}_{\alpha,\beta}) * (W^{p}_{\alpha,\beta}) \end{aligned} \tag{5}$$

where p and q take the values a and b. Up to now, there are no precise calculations available from the structure and we shall make a choice of the relative weights consistent with the symmetry. Varying the relative weights gives slight differences [33] in the energies which for the moment can be considered refinements of the gross features. In practice we shall choose the exchange $J_{\rm a}$ between the moments a to be J_0 with the two nearest (α and β) BETS orbitals i and zero otherwise, the exchanges $J_{\rm b}$ being then determined by inversion symmetry. Hence, the exchange depends on a single exchange parameter J_0 to be compared with experiment. Unlike the situation of a single band for which

$$\chi_{\rm tot}(Q) = \sum_{\alpha}\chi_{\alpha,\alpha}(Q) \tag{6}$$

there is a significant difference with the magnetic susceptibility of the present conduction bands in that the non-diagonal elements $\chi_{\alpha,\beta}$ with $\alpha \neq \beta$ are important. Thus the wave vector $\mathbf{Q}$ favoured for magnetic order in general bears no relation with that for the correlations-induced instabilities towards charge or spin density waves in a single conduction band only. Physically this is because the magnetic moments interact *via* virtual pairs of electrons and holes and, since the exchange interaction is not diagonal in band index, there is no reason why the band indices of the electron and the hole should be the same. In contrast, when we calculate the total non-interacting susceptibility of a single conduction band there is no term in the Hamiltonian that changes the band index so only the diagonal parts of χ contribute. For instabilities the optimal wavevector depends on the detailed structure of the correlation terms but in the simplest cases the vector is determined by the maximum of the total susceptibility [34].

Such a model enables us to calculate numerically the RKKY exchange. We find that the position of the maximum is in fact determined primarily by the off-diagonal term $\chi_{1,2}$ describing the virtual excitation of an electron from the primarily filled highest band 1 with a hole from the primarily empty next band 2. The $\mathbf{Q}$ vector that maximizes $\chi_{1,2}$ is that which best transposes the electron sheet to the hole tube. Thus if a simple geometric picture is to be applied to guess the magnetic order, it involves translating the two partially occupied surfaces with respect to each other rather than looking for nesting properties of individual surfaces. Detailed calculations [33] including contributions from all four bands lead to the following exchange for magnetic order

$$\begin{aligned} J(\mathbf{Q}) =& \frac{J^{\rm aa}(\mathbf{Q}) + J^{\rm bb}(\mathbf{Q})}{2} \\ &+ \sqrt{\frac{[J^{\rm aa}(\mathbf{Q}) - J^{\rm bb}(\mathbf{Q})]^2 + 4[J^{\rm ab}(\mathbf{Q})]^2}{4}}\,. \end{aligned} \tag{7}$$

For the parameters we took, this gave a maximum in $J(\mathbf{Q})$ at $\mathbf{Q} = (0.98c^*, -0.16a^*)$ with an exchange $J(\mathbf{Q}_{\rm max}) = J_0^2$ (80 $({\rm eV})^{-1}$). Since the spins are well defined and rather large we would then predict a helical order with this incommensurable turn angle. Nevertheless, including a weak magnetic order with this $\mathbf{Q}$ vector, while it would cause partial reconstruction of the FS, it is unable to suppress the entire FS of Figure 2, as experimentally realized.

In order to understand the transport properties of $\lambda-$BETS, we have to go beyond simple RKKY and include the effect that magnetic order will have back on the Fermi surface. The exchange term in the Hamiltonian (1) is treated on an equal footing to the conduction part of the Hamiltonian, which is generally a very difficult many-body problem. However, since a stable magnetic order is realized in the ground state, the localised spins will be treated as classical vectors, *i.e.* without transverse fluctuations around an assumed ordering direction of their large $S = 5/2$ moment. Although we neglect these quantum fluctuations of the iron moments, we do treat the spin fluctuations on the conduction electrons. This approach is very similar to that of Hamada and Shimahara [35] for simpler Kondo lattice model problems. Our current objective is to present a plausible mechanism for the magnetic and transport properties. So we neglect in first approximation spin wave corrections to the classical order and coupling between the latter and charge fluctuations. The transport properties are affected by the static spin order since the conduction electrons experience a spin-dependent Hamiltonian which varies from unit cell to unit cell of the original non-magnetic structure. It is clear, however, we have to be rather careful about quantitative

comparisons: for example, as the compound is highly 2D, thermal fluctuations of spin waves in any ordered state will reduce the ordering temperature significantly. The precise value of the ordering vector is sensitive to the band structure as well as the approximations used, but we aim to explain bulk properties that are currently measurable.

With such reservations, we proceed and use the ideas of the RKKY calculation as a guide to magnetic structures but we go beyond the RKKY calculation in that we treat the change of Fermi surface and the different magnetic order in a self-consistent way. We take the Hamiltonian, freeze in a pure helical order, *i.e.* with a wave-vector for uniform turn angles, to keep the Hamiltonian translationally invariant in the rotating frame and then recalculate in this new frame the band structure, the Fermi energy and total kinetic energy by summing over the occupied states [34].

We have carried out this procedure to see i) the effect of helical order on the electronic structure and ii) whether or not we can explain the metal-insulator transition by this mechanism. First we consider the case with $U = 0$, looking only at ordering vectors close to the vector predicted for the maximum in the RKKY interaction. A more exhaustive study will be published elsewhere [33]. The main result of this calculation is that if we stay at the wave vector predicted perturbatively in coupling J_0, as we increase the value of J_0 there is reconstruction of the Fermi surface. This reconstruction diminishes the number of carriers, and for J_0 greater than about 6 meV there is a metal- insulator transition, *i.e.* the system becomes a helically ordered insulator.

As the crystals cannot be grown of sufficient size, this prediction of an insulator induced by a form of helical antiferromagnetism cannot be tested directly by neutron diffraction. Nevertheless this seems in good agreement with the present magnetic measurements. In applied magnetic field we would expect a heli-fan since the spins are taken isotropic: *i.e.* we take the same wave-vector but allow the spins to rotate perpendicularly to the magnetic field with a component constant and parallel to the field. The spin S^{a} or S^{b} (always considered to be classical) has components

$$\mathbf{S}(i) = (S\sin(\alpha)\cos(\mathbf{Q}\cdot\mathbf{r}_i + \beta_0), \\ S\sin(\alpha)\sin(\mathbf{Q}\cdot\mathbf{r}_i + \beta_0), S\cos(\alpha)) \quad (8)$$

where α is the canting angle and i runs over the set of all equivalent iron moments. For the sake of simplicity we consider only states where the canting angle and phase β_0 are the same for the two set of spins. With such a heli-fan structure we can recalculate the band structure and then the total energy with a field dependent term

$$2g_{\mathrm{Fe}^{3+}}m_{\mathrm{B}}SB\cos(\alpha) + g_e m_{\mathrm{B}}\langle\mathbf{s}_i\rangle\cdot\mathbf{B} \quad (9)$$

where $\langle\mathbf{s}\rangle\cdot\mathbf{B}$ is calculated from the renormalized band structure. $\langle\mathbf{s}\rangle$ is the expectation value of the spin from the conduction bands per unit cell. Clearly as the field increases these terms favour a heli-fan and ultimately a fully aligned paramagnetic state. In Figure 18, we show the reconstructed Fermi surface for $\alpha = 0.3\pi$ and the parameter $J_0 = 8$ meV. For α smaller than 0.35π, the Fermi surface reappears. Thus the magnetic field, by aligning the iron moments, diminishes the effect of the exchange coupling and restores a conducting state with small closed orbits, the area of which being very similar to that experimentally measured (2% of the first BZ).

Thus in principle we have a mechanism to allow for an insulating state and restoration of the conduction at finite field. We can now go deeper and consider whether or not the values of the coupling are reasonable, both from a microscopic point of view and in view of our experiments. First, in order to account for the occurrence of the insulating phase at zero field we invoked a coupling of 8 meV. This in turn implies a Néel temperature, from an RKKY estimate of $80 \times (0.008)^2 = 0.005$ eV, which is rather larger than the temperature deduced from experimental data $T_{\mathrm{N}} \sim 8$ K. As previously argued, we do not expect exact agreement with the RKKY expression, since the exchange interaction modifies the Fermi surface and, as the Fermi surface disappears, the susceptibility should decrease from the RKKY estimate. Moreover, if we include a nonzero correlation energy U, which we expect to be relatively large, we should consider not only the magnetic instabilities involving the iron moments but also the competing instabilities within the bands. Numerically, the effect of introducing correlations within a Hartree-Fock approximation is to reduce the value of exchange needed to give an insulating state in zero field. This may also account for part of the discrepancy between the Néel temperature and the gap.

As a check on the magnitudes of the couplings we can compare the energy difference ΔE of an insulating state $\alpha = 0.5\pi$ for $J_0 = 8$ meV and that of a fully aligned paramagnetic conducting state $\alpha = 0$. Our numerical calculations yield $\Delta E = 0.0005$ eV $= g\mu S B_{\mathrm{c}}$ with $g = 2$, $S = 5/2$, $\mu = 1.2 \times 10^{-4}$ eV/T corresponding to a critical field $B_{\mathrm{c}} = 1$ T. This estimate, to be compared to the experimental value of about 10 T, is very crude but shows that the orders of magnitude are correct. Since the energies of different ordered states are small it is likely, as spin-flop transition is experimentally observed, that this could lead to a sequence of states of different canting angles at low temperatures.

5 Conclusion

In conclusion, the anisotropic properties of the static (SQUID) and dynamic (ESR, AFR) magnetization measurements we have performed upon both polycrystalline sample and single crystals, sign without ambiguity the AF character of the insulating state of λ−$(\mathrm{BETS})_2\mathrm{FeCl}_4$. The first order character of the metal-insulator transition curve $T_{\mathrm{N}}(B)$ has been simultaneously established through cantilever and magnetoresistive measurements in steady fields. In the low magnetic field part of the phase diagram, the easy axis of magnetization is close to the c crystallographic axis. A "spin-flop" transition line sets apart this ground state from a field induced canted AF. The magnetism of this compound is likely dominated by the

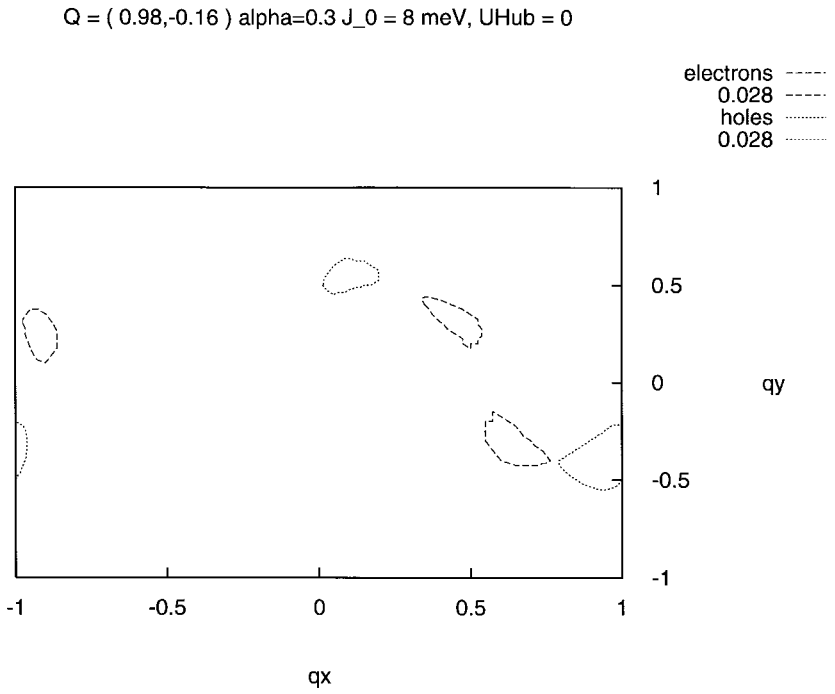

Fig. 18. Reconstructed Fermi surface of $\lambda-(BETS)_2FeCl_4$ for $\alpha = 0.3\pi$, $J_0 = 8$ meV, $U = 0$ (see text) and $\mathbf{Q} = (0.98c^*, -0.16a^*)$. Electron and hole pockets are cut for an energy equal to 28 meV.

indirect exchange between the localised moments of the $S = 5/2$ Fe^{3+} ions, which stack along 1D chains parallel to the c axis. These moments, which are screened by the Cl^- ions, polarise in turn the 2D carriers spins of the BETS molecules in the intercalated ac sheets. We have modelled this generalized Kondo lattice by a Hubbard Hamiltonian taking into account i) indirect exchange through RKKY interactions, ii) correlations within the Hartree-Fock approximation and iii) Zeeman terms, the effect of which being simulated by canting of the iron moments. Although transverse fluctuations of these moments are neglected, calculations show that this model yields a field induced transition between a low field, low temperature AF insulating state and a metallic state which is not a fully oriented paramagnetic state but still presents some rest of canting. Although it cannot account for all the complexity of the experimental phase diagram, namely the "spin-flop" transition, this model of a helically ordered insulator undergoing an insulator to metal transition at finite field appears to be consistent with the experimental results.

It is a pleasure to thank M. Kurmoo, E. Coronado and D. Bertrand for interesting discussions on magnetic phase transitions and metamagnetism.

References

1. For a recent review, see *Common Trends in Synthetic Metals and High-T_c Superconductors*, D. Jérome, J. Phys. France I **6**, 12 (1996).
2. R. Kato, H. Kobayashi, A. Kobayashi, Y. Sasaki, Chem. Lett. 1693 (1984).
3. P. Batail, L. Ouabab, J.B. Torrance, M.L. Pylman, S.S.P. Parkin, Sol. Stat. Comm. **55**, 597 (1985).
4. R. Kato, H. Kobayashi, A. Kobayashi, Synth. Met. **41-43**, 2093 (1991).
5. T. Naito, A. Miyamoto, H. Kobayashi, R. Kato, A. Kobayashi, Chem. Lett. 1945 (1991).
6. H. Kobayashi, T. Udagawa, H. Tomita, K. Bun, T. Naito, A. Kobayashi, Chem. Lett. 1559 (1993).
7. A. Kobayashi, T. Udagawa, H. Tomita, T. Naito, H. Kobayashi, Chem. Lett. 2179 (1993).
8. A. Kobayashi, R. Kato, T. Naito, H. Kobayashi, Synth. Met. **55-57**, 2078 (1993) .
9. H. Kobayashi, H. Tomita, T. Udagawa, T. Naito, A. Kobayashi, Synth. Met. **70**, 867 (1995).
10. H. Kobayashi, H. Tomita, T. Naito, A. Kobayashi, F. Sakai, T. Watanabe, P. Cassoux, J. Am. Chem. Soc. **118**, 368 (1996).
11. L.K. Montgomery, T. Burgin, J.C. Huffman, J. Ren, M.H. Whangbo, Physica C **219**, 490 (1994).
12. H. Kobayashi, A. Kobayashi, International Symposium on Crystalline Organic Metals, Superconductors and Ferromagnets (Sesimbra Portugal March 22-27, 1997).
13. M. Kurmoo, A.W. Graham, P. Day, S.J. Coles, M.B. Hurtsthouse, J.M. Caufield, J. Singleton, L. Ducasse, P. Guionneau, J. Am. Chem. Soc. **117**, 12209 (1995).
14. S. Turner, L. Martin, P. Day, International Symposium on Crystalline Organic Metals, Superconductors and Ferromagnets (Sesimbra Portugal March 22-27, 1997).
15. D. Jérome, H.J. Schulz, Advances in Physics **31**, 299 (1982); D. Jerome, Solid State Comm. **92**, 89 (1994).
16. F. Goze, V.N. Laukhin, L. Brossard, A. Audouard, J.P. Ulmet, S. Askenazy, T. Naito, H. Kobayashi, A. Kobayashi, M. Tokumoto, P. Cassoux, a) Europhys. Lett. **28**, 427 (1994); b) Synth. Met. **71**, 1901 (1995).
17. M. Chaparala, O.H. Chung, M.J. Naughton, AIP Conf. Proceed. **273**, 407 (1992); M.J. Naughton, Phys. Today **3** (1996).
18. D. Chasseau, private communication.

19. J.H. Ammeter, H.B. Burgi, J.C. Thibeault, R. Hoffmann, J. Am. Chem. Soc. **100**, 3686 (1978).
20. M. Tokumoto, T. Naito, H. Kobayashi, A. Kobayashi, V.N. Laukhin, L. Brossard, P. Cassoux, Synth. Metals **86**, 2161 (1997).
21. A. Perez-Benitez, C. Rovira, J. Veciana, V.N. Laukhin, E. Molins, J. Vidal-Gancedo, A. Cabrero, I. Mata, C. Jimenez, E. Coronado, International Symposium on Crystalline Organic Metals, Superconductors and Ferromagnets (Sesimbra Portugal March 22-27, 1997).
22. C. Coulon, J.C. Scott, R. Laversanne, Phys. Rev. B **33-9**, 6235 (1986).
23. T. Nagamiya, Prog. Theor. Phys. **11-3**, 309-327 (1954); T. Nagamiya, K. Yosida, R. Kubo, Adv. Phys. **4-13**, 1-112 (1955).
24. C. Coulon, R. Laversanne, J. Amiell, Physica B **143**, 425 (1986).
25. D. Bloch, J. Voiron, J.C. Bonner, J.W. Bray, I.S. Jacobs, L.V. Interrante, Phys. Rev. Lett. **44**, 294 (1980).
26. C. Coulon, R. Laversanne, J. Amiell, Physica **143B**, 425 (1986).
27. I.S. Jacobs, P.E. Lawrence, Phys. Rev. **164**, 866 (1967).
28. D.P. Landau, B.E. Keen, B. Schneider, W.P. Wolf, Phys. Rev. B **3**, 2310 (1971); M. Blume, L.M. Corliss, J.M. Hastings, E. Schiller, Phys. Rev. Lett. **32**, 544 (1974).
29. H.J.M. de Groot, L.J. de Jongh, Physica **141B**, 1 (1986).
30. T. Tiedje, J.F. Carolan, A.J. Berlinsky, L. Weiler, Can. J. Phys. **53**, 1593 (1975); G. Bonfait, E.B. Lopes, M.J. Matos, R.T. Henriques, M. Almeida, Solid State Commun. **80**, 391 (1991); C. Bourbonnais, R.T. Henriques, P. Wzietek, D. Kögeter, J. Voiron, D. Jérome, Phys. Rev. B **44**, 641 (1991).
31. J.W. Bray, L.V. Interrante, I.S. Jacobs, J.C. Bonner, in *Extended Linear Chain Compounds*, Vol.3, edited by J.S. Miller (Plenum Press, NY and London, 1983).
32. S. Doniach, Physica B **91**, 231 (1977); R. Julien, J.N. Fields, S. Doniach, Phys. Rev. B **16**, 4889 (1977); L.G. Caron, C. Bourbonnais, Europhys. Lett. **11**, 473 (1990).
33. T. Ziman, to be published.
34. M. Gusmao, T. Ziman, Phys. Rev. B **54**, 16663 (1996).
35. Hamada, Shimahara, J. Phys. Soc. Jpn **65**, (1996) 552.